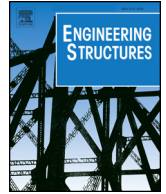




ELSEVIER

Contents lists available at ScienceDirect

Engineering Structures

journal homepage: www.elsevier.com/locate/engstruct

FE simulation of cylindrical RC containment structures under reserved cyclic loading

Hieu Cong Luu^{a,*}, Y.L. Mo^b, Thomas T.C. Hsu^b, C.L. Wu^c

^a Department of Infrastructure, RPS, Houston, TX 77079, USA

^b Department of Civil and Environmental Engineering, University of Houston, Houston, TX 77204, USA

^c National Center for Research on Earthquake Engineering, Taipei 10668, Taiwan

ARTICLE INFO

Keywords:

Reinforced concrete
Nuclear containment structures
Shell element, constitutive model
Nonlinear finite element

ABSTRACT

The nuclear containment structure is one of the most important infrastructure systems ensuring the safety of a nuclear power plant. The structural behavior of a cylindrical containment structure made of reinforced concrete (RC) with large dimensions and numerous rebars is complex and difficult to predict. The complex behavior of the RC containment structure has been investigated in an international collaboration project between the National Center for Research on Earthquake Engineering (NCREE) in Taipei, Taiwan and the University of Houston (UH), Houston, Texas. At NCREE two 1/13 scaled cylindrical RC containment specimens were tested under reversed cyclic loads [1]. At UH, a finite element simulation of the two tested specimens was developed using a finite element analysis (FEA) program SCS [2]. In the program, a new shell element, the so-called CSMM-based shell element, was developed based on the Cyclic Softened Membrane Model [3] and the formulation of an 8-node Serendipity curved shell element [4] with a multi-layer approach [5]. The UH simulated seismic behavior was close to the NCREE experimental results. This paper presents the theoretical development of the FEA program SCS and the comparisons of its predictions with the experimental structural behavior of the two RC containment specimens. This simulation model and the FEA program are excellent tools to develop effective performance-based design provisions.

1. Introduction

The safety of a nuclear power plant depends strongly on its containment structure. A nuclear containment structure is commonly a steel or reinforced concrete structure enclosing a nuclear reactor. This structure serves as a barrier to prevent various types of harmful radiation from contaminating the atmosphere during a rare nuclear meltdown accident [6]. Because of its critical importance to nuclear safety, the nuclear containment structure must be able to maintain structural integrity while undergoing simultaneous stresses caused by internal pressure, earthquake action and/or high local loads [7]. Considered to be a competitive material that satisfies safety requirements, reinforced concrete (RC) has been used for the nuclear containment structure since the beginning of the nuclear power industry [8]. The structural behavior of the RC nuclear containment structure with large cross sections, many layers of rebars, and complex stress conditions, is difficult to predict, especially when subjected to the earthquake loading. The seismic response of the RC nuclear containment structures is highly nonlinear caused by the highly inelastic behavior of materials

including rebars and concrete under reversed cyclic actions. However, from the structural point of view, a whole RC nuclear containment structure can be visualized as assemblies of many RC elements so that the finite element analysis program combined with proper constitutive models for concrete and reinforcing bars can be a very powerful tool. The key to rational analyses of the RC nuclear containment structure is to completely understand the behavior of one element isolated from the structure. Once a rational model is developed to predict the behavior of one element, this model can be incorporated into a finite element analysis program to predict the behavior of the whole structure under different kinds of loading.

To predict the response of the RC nuclear containment structure under severe loading, researchers need to use accurate material models and efficient numerical tools. In general, lumped-mass stick models and finite element models are two methods commonly used for the analysis modeling of the nuclear containment structure [6]. Many researchers have used finite element method to predict the behavior of RC nuclear containment structures. The main approach is to consider the RC nuclear containment as a shell-type structure and to use an appropriate

* Corresponding author.

E-mail address: hclu@uh.edu (H.C. Luu).

shell element to simulate its behavior. The reinforced concrete shell element is often developed by combining a constitutive model of reinforced concrete material into finite element formulations of a general shell element with layer approaches (Hand, Pecknold [9]; Cervera, Hinton [10]; Hu and Schnobrich [11]; Yamamoto and Vecchio [12]; Kim, Lee [13]; Maekawa, Okamura [14]; Zhang, Bradford [15]; and Lee [16]). The studies of the researchers show that a selection of appropriate material models, which provides adequate accuracy with reasonable computational time, plays an important role in the success of the analysis of the RC shell-type structures using the finite element method.

The main problems faced by most of the researchers in the analysis of RC nuclear structures are that the finite element analysis often requires extensive computational time due to the complicated material models and the difficulties encountered in the stability and accuracy of the solutions. Some material models for reinforced concrete material, such as fracture mechanics or detail crack localizations, were successfully verified at the element level but faced numerical problems when applied to the structure level, which requires a large number of elements. In recent years, the smeared-crack concept has been widely used in the analysis of RC structures. The concept allows the internally-cracked reinforced concrete composite to be treated as a simple, continuous material rather than a complicated, discontinuous composite [17]. The advantage of this simplification is that mechanics-based analysis can be applied to predict the behavior of the RC shell structures regardless of cracking. To implement this simplification, the material constitutive models must be based on the smeared (averaged) stress and strain relationship of the internally cracked RC elements. Since the 1980s, many researchers have conducted studies of the constitutive material of reinforced concrete based on the smeared-crack concept; however, only a few research groups could conduct an experimental study of shell elements [18,19]. Using the experimental results of RC panel tests, many constitutive models for RC have been proposed including the Compression-Field Theory and the Modified Compression Field Theory [20], the Rotating-Angle Softened Truss Model (RA-STM) [21,22], the Fixed-Angle Softened Truss Model (FA-STM) [23], the Softened Membrane Model (SMM) [24] and the Cyclic Softened Membrane Model (CSMM) [3]. Among these constitutive models, the CSMM (Fig. 1) is the most versatile and accurate and is capable of rationally predicting the cyclic shear behavior of reinforced concrete elements including the stiffness, ultimate strength, descending branch, ductility and energy dissipation capacity.

Over the past several decades, researchers at the University of Houston have made significant contributions on the finite element analysis of RC elements and members subjected to shear. Zhong [25] developed a nonlinear finite element computer program, the Simulation of Concrete Structures (SCS), using the OpenSees framework [26]. In the program, a two-dimensional reinforced concrete plane stress membrane element was developed based on the Cyclic Softened Membrane Model to simulate the behavior of reinforced concrete shear walls subjected to static, reversed cyclic and dynamic loading. Recently, Luu, Mo [2] implemented a new shell element, the so-called CSMM-based shell element, into the SCS program. The element was developed based on the Cyclic Softened Membrane Model [3] and the formulation of an 8-node Serendipity curved shell element [4] with a layered approach [5]. The developed CSMM-based shell element successfully predicted the structural behavior of several types of three-dimensional RC structures, such as a RC cylindrical tank, and circular and rectangular RC hollow bridge piers.

The purpose of this paper is to validate the capacity of the developed CSMM-based shell element to simulate the cyclic response of nuclear containment structures using the test results of two 1/13-scaled RC nuclear containment vessel (RCCV) specimens subjected to reversed cyclic loads [1]. The tests were undertaken as part of an international collaboration project between the National Center for Research on Earthquake Engineering (NCEE) in Taipei, Taiwan and the University

of Houston (UH), Houston, Texas. This paper provides: (1) the development and implementation of the CSMM-based shell element and the theoretical development of the FEA program SCS in OpenSees; (2) brief descriptions of the test program, test specimens, test setup and loading method; and (3) the nonlinear analysis of the containment specimens using the FEA program SCS with the CSMM-based shell element. Results from the study provided a critical connection between the simulation models and the actual experimental structural behavior of the RC nuclear containment structures. Detailed descriptions of the reversed cyclic tests are given in a paper authored by the nuclear energy research team of NCEE [1].

2. Description of CSMM-based shell element

In this section, the description of the CSMM-based shell element presented in the recent work by the authors is briefly recalled since it serves as the most important aspect needed to the comprehension of the subsequent sections. The CSMM-based shell element was developed by utilizing the formulation of an 8-node Serendipity curved shell element [4]. The Serendipity shell element has a total of eight nodes with five degrees of freedom (DOF) at each node, three translational DOFs and two rotational DOFs (Fig. 2). The Serendipity shape function was applied to all DOFs. The element showed excellent performance when applied to the cases of moderate thick shell structures by using the standard full integration rule [27]. The idea of creating the element arose from the difficulty of solving the ill-conditioned equations that occurred in the three-dimensional solid element when the dimension in the thickness direction was small. Therefore, it is also referred to as a degenerated curved shell element [4]. The degenerated curved shell element with the layered approach has been recognized as one of the most effective and reliable methods for analysis of RC shell-type structures since the 1970s [27,28].

By using the degenerated curved shell element with the layered approach, the behavior of RC shell structures can be captured directly from the cyclic stress-strain relationships of the materials, and no phenomenological rule is needed [11]. The element was derived from the equations of three-dimensional continuum mechanics by reducing their dimensions in the thickness direction and was based on the Reissner-Mindlin theory, which only requires C0 continuity in the shape function for assuring complete inter-element deformation compatibility and can model the behavior of reinforced concrete shells with significant transverse shear deformation. The local material stiffness matrix of the shell element was derived based on the layered approach given by Scordelis and Chan [5], in which the section of the shell element can be divided into several layers throughout the thickness (Fig. 3). The strains at each layer are assumed to be uniform and interpolated by shape functions from the displacements at all nodes of the element. The detailed presentation of the finite element formulation of the shell element is available elsewhere [29].

2.1. Constitutive material model

The constitutive model used in the CSMM-based shell element was based on the Cyclic Softened Membrane Model proposed by Mansour and Hsu [3], as shown in Fig. 1. The model is capable of accurately predicting the pinching effect, the shear ductility and the energy dissipation capacities of RC members. CSMM included the cyclic uniaxial constitutive relationships of concrete and embedded mild steel. The characteristics of these concrete constitutive laws include (1) the softening effect on the concrete in compression due to the tensile strain in the perpendicular direction; (2) the softening effect on the concrete in compression under reversed cyclic loading and (3) the opening and closing of cracks, which are taken into account in the unloading and reloading stages. The characteristics of embedded mild steel bars include (1) the smeared yield stress is lower than the yield stress of bare steel bars and the hardening ratio of steel bars after yielding is

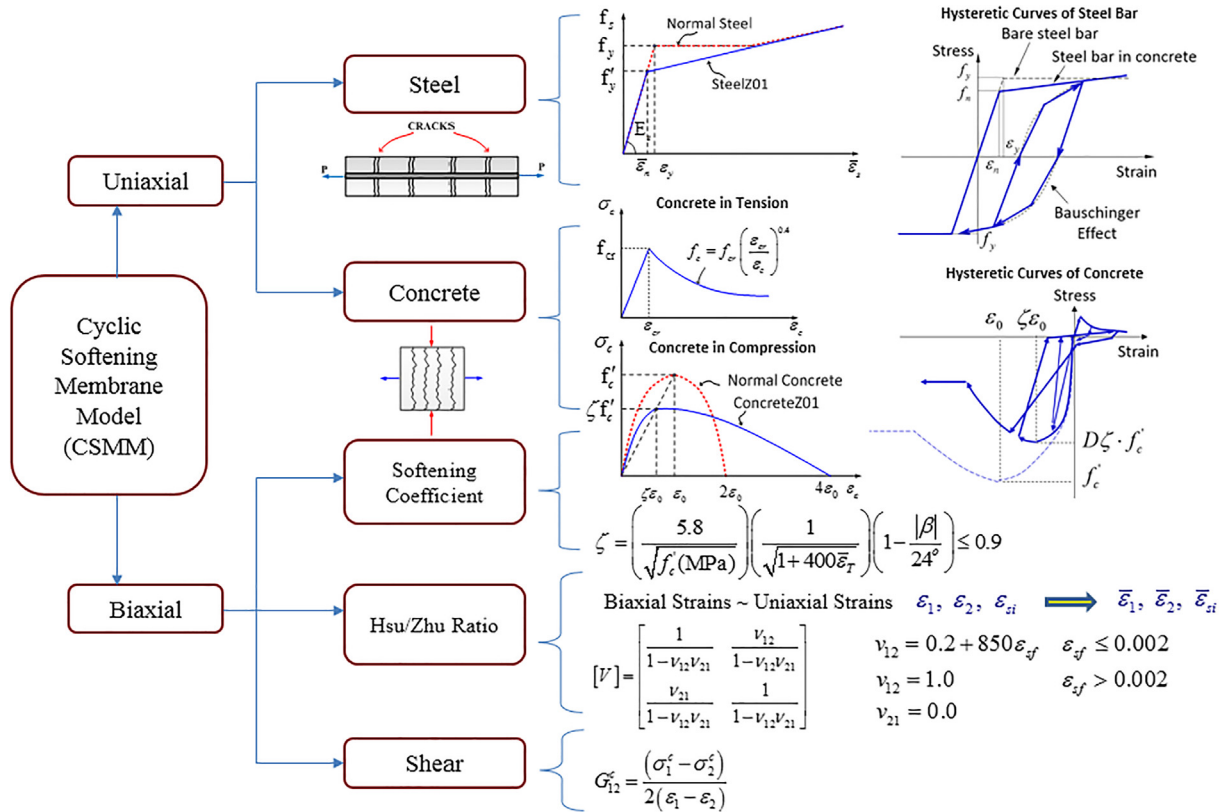


Fig. 1. Overview of Cyclic Softening Membrane Model for reinforced concrete.

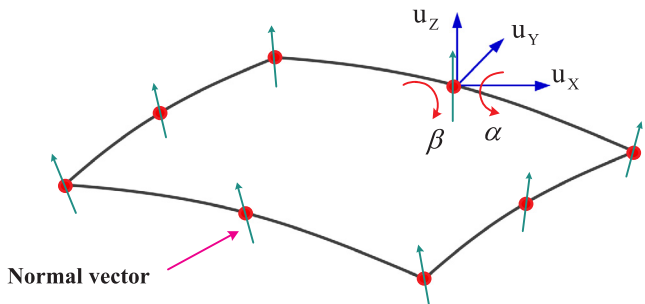


Fig. 2. Eight-node degenerated shell element.

calculated from the steel ratio, steel strength and concrete strength and (2) the unloading and reloading stress-strain curves of embedded steel bars take into account the Bauschinger effect.

2.2. Analysis procedure

An analysis procedure was developed to perform nonlinear analyses of RC nuclear containment structures using the developed CSMM-based shell element. Fig. 4 shows a flow chart for the analysis solutions under load increment. Throughout the procedure, the tangent material matrix $[\bar{D}]$ was determined first, and the element stiffness matrix $[k^e]$ and the element resisting force increment vector $\{\Delta f\}$ were calculated. Then the global stiffness matrix $[K]$ and global resisting force increment vector $\{\Delta F\}$ were assembled. In each iteration, the tangent material matrix $[\bar{D}]$, the element stiffness matrix $[k^e]$ and the global stiffness matrix $[K]$ were iteratively refined until a convergence criterion was achieved.

In the analysis, in order to establish the constitutive material matrix at each layer of the CSMM-based shell element, the principal stress direction θ_1 was evaluated at the cracking loading step and was maintained during the analysis. Once the principal stress direction θ_1 was defined, the local material matrix of each layer $[D_{layer}]$ could be obtained at each layer of the shell element. The outer white block in Fig. 4 outlines the procedure for the calculation of the element stiffness and the element resisting force of the shell elements. This algorithm utilized

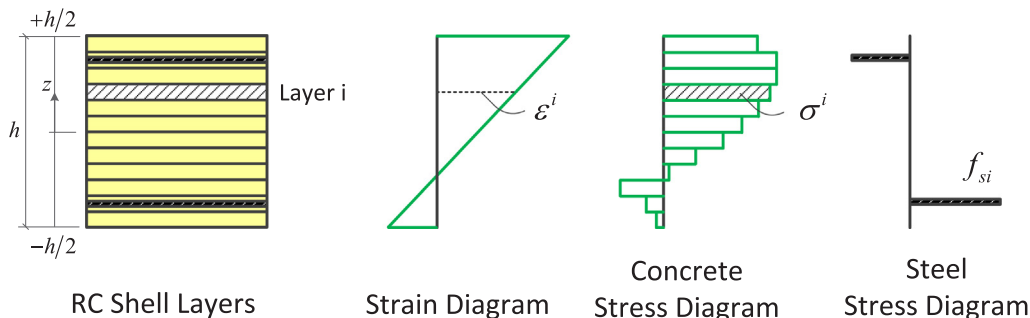


Fig. 3. Concept of layered approach.

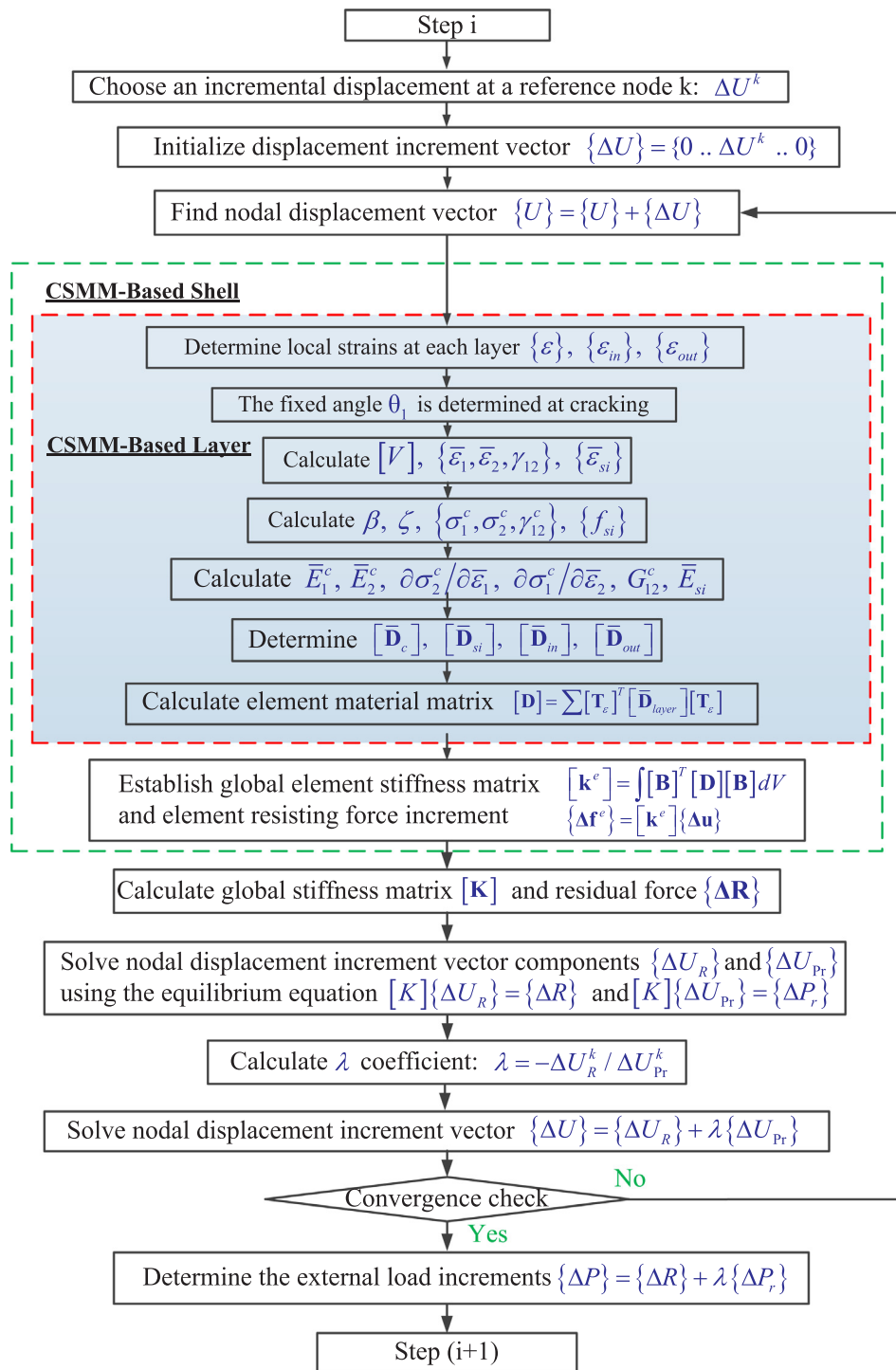


Fig. 4. Analysis procedure for the CSMM-based shell element.

the Newton-Raphson method with displacement control originally proposed by Batoz and Dhat [30]. The tangent material matrix $[D]$, the element stiffness matrix $[k^e]$ and the global stiffness matrix $[K]$ were calculated in each iteration.

2.3. Implementation

New modules that represent the proposed element and materials were implemented into the OpenSees framework to create a finite element analysis program, Simulation of Concrete Structures (SCS) [29]. OpenSees stands for Open System for Earthquake Engineering

Simulation. OpenSees was developed in the Pacific Earthquake Engineering Center (PEER) and is an object-oriented framework for simulation applications in earthquake engineering using finite element methods [26]. The implementation of the developed modules into OpenSees is shown in Fig. 5. Fig. 5 presents only the ModelBuilder, while the Analysis and Recorder objects are omitted. The element module CSMMShellS8 represents the CSMM-based shell element. The nDMaterial module CSMMLayer was created to incorporate the formulation of the tangential material matrix for concrete and steel into each layer of the developed shell element. The CSMMLayer was connected with the two uniaxialMaterial modules, SteelZ01 and

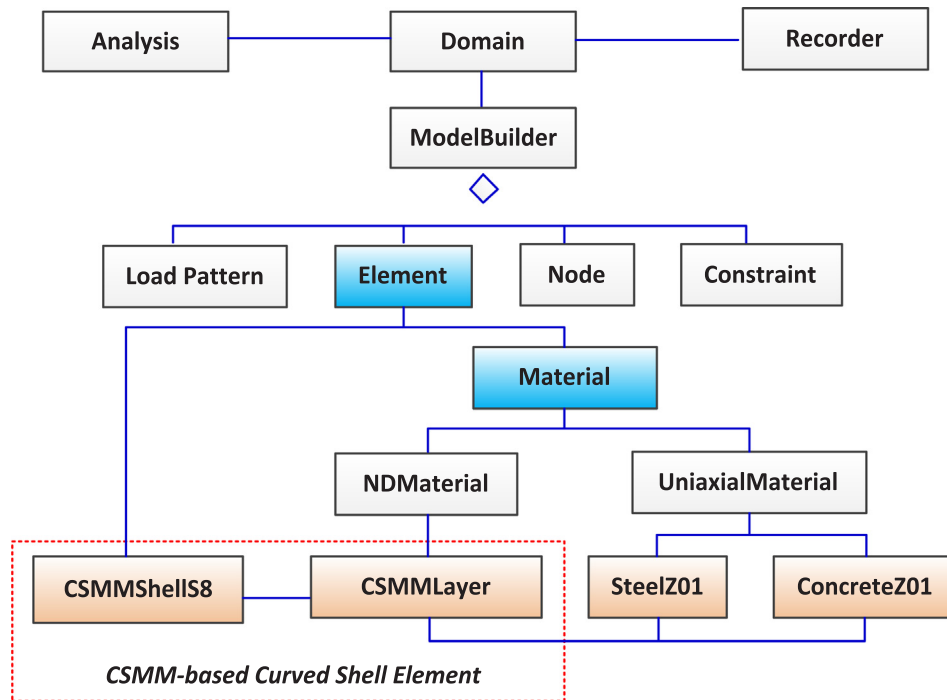


Fig. 5. Implementation of the SCS program in OpenSees framework.

ConcreteZ01, to determine the material constitutive matrix and calculate the stress of the elements at each layer. Two uniaxialMaterial modules for concrete (ConcreteZ01) and steel (SteelZ01) were created previously based on the uniaxial constitutive relationship of concrete and steel in CSMM [25].

3. Simulation of RC nuclear containment structures

3.1. Description of test program

The experimental program included the construction and testing of two 1/13-scaled nuclear containment specimens. These specimens were designed to investigate the behavior of a RC nuclear containment isolated from a nuclear power plant and subjected to the gravity and earthquake loads. The specimens were designed based on the prototype of an Advanced Boiling Water Reactor (ABWR) nuclear containment structure (Fig. 6a). The real-size containment has a height of 29.5 m, a radius of 15.5 m (center-line dimension) and a thick wall of 2.0 m (Fig. 6b). Each specimen included three parts: the main containment, top block and bottom block. The bottom block simulated the rigid foundation while the top block simulated the rigid floor system. These blocks were designed with steel plate boxes filled with concrete and a large amount of reinforcing steel. These blocks were designed conservatively to avoid significant deformation occurring in the blocks so that the nonlinearity occurred only in the containment walls during the tests. Rotations of the top and bottom blocks in the vertical plane were prevented during the test to ensure the containments deforming in a double-curvature manner during the tests. The dimensions of the test specimens are shown in Fig. 7. The containments had a height of 2.25 m and a radius of 1.175 m (centerline dimension). The outer and inner diameters of the containments were 2.5 m and 2.2 m, respectively. Thickness of the containment was 0.15 m. The top and bottom blocks of the specimens had a cross section of 3.5 m × 3.5 m and a depth of 0.73 m.

The reinforcement arrangement in the specimens is illustrated in Fig. 8. Four layers of vertical and horizontal steel rebars were uniformly placed along the thickness of the containments. The steel rebars were uniformly distributed around the perimeter and along the height of the

test containments with the same spacing. The percentage of the reinforcement ratio in the containment of Specimen No. 1 was 2% in both the vertical and horizontal directions (Fig. 8a). The reinforcement arrangement of Specimen No. 2 was almost identical to Specimen No. 1 except that more vertical steel rebars (dowel bars) were added to each end of the containment to enhance its shear sliding capacity, resulting in the vertical reinforcement ratio of 4% in each of these two ends (Fig. 8b). The cut-off points of the additional vertical steel rebars were arranged in a jagged manner to prevent cracking within the cut-off regions. The centerline of the zigzag curve was at a quarter of the containment height. The vertical bars in the containments were continuous without lap splices. The clear concrete cover over the vertical bars was 17 mm. The details of dimensions and material properties of the specimens are summarized in Table 1. The compressive strengths of concrete of Specimen No. 1 and Specimen No. 2 at the testing date were 37.0 MPa and 43.3 MPa, respectively. Both specimens used the same steel bars taken from the same batch. The yielding strength of the vertical and horizontal steel bars was 379 MPa and 376 MPa, respectively.

At the NCRE Laboratory in Taiwan, the test specimens were subjected to horizontal loading up to their maximum capacity with a set of specially built steel loading frames. The test setup was used to simulate gravity and the lateral and vertical earthquake loads. Fig. 9 gives an overview of the test setup with various equipment components, including the horizontal actuators, vertical actuators, L-shape steel loading frame systems and the specimen. The specimens were loaded axially using four 1000-kN-capacity vertical hydraulic actuators. Pin connections were used at the end of the vertical actuators. The simulated lateral earthquake load was applied by eight 1000-kN-capacity horizontal actuators under displacement control. The horizontal actuators were bolted to a rigid concrete reaction wall and the L-shape loading frame so that the center of the loading axis passed through the specimen's mid-height. The specimens were connected to the strong concrete floor using high-strength all-thread steel rods that went through the foundation of the specimens. The loading frame was allowed to move freely in the vertical plane. Additional steel frames bolted to the solid floor were placed on the north and south sides of the specimen to prevent the horizontal out-of-plane displacement. During

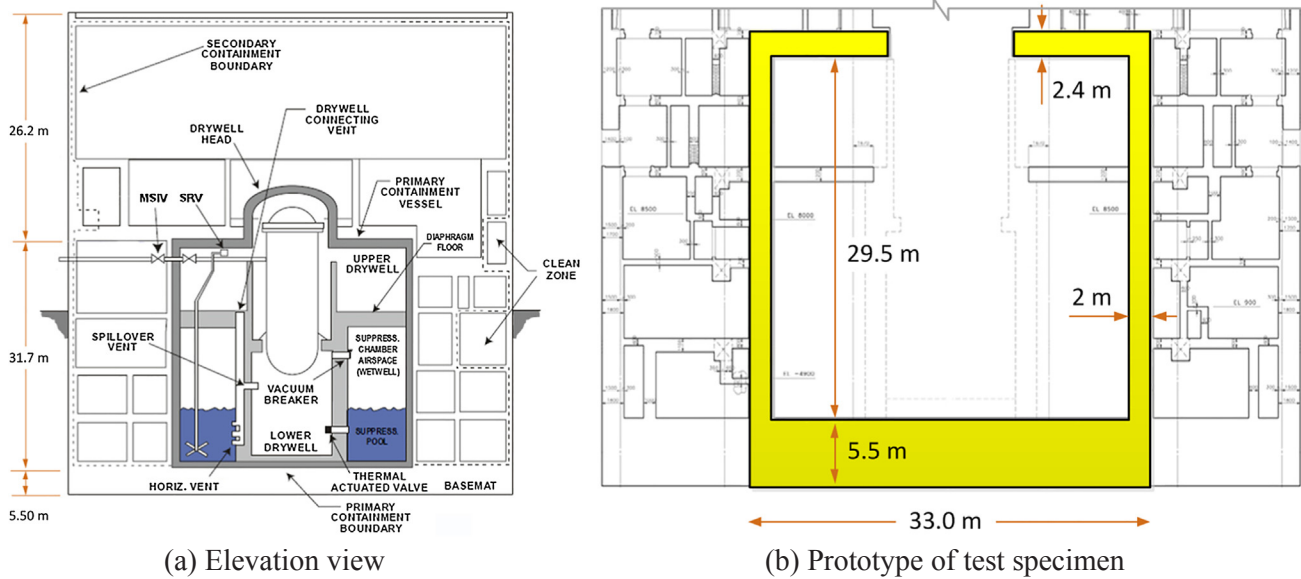


Fig. 6. ABWR nuclear power plant.

the tests, the containment specimens were subjected to constant vertical axial loads and horizontal reversed-cyclic load until failure.

The first step of the loading protocol program was to apply an axial load that would remain constant during the course of the test. The total initial vertical load equaled 1.6% of the axial concrete capacity ($f'_c A_g$) of each specimen, where f'_c is the compressive strength of concrete and A_g is the nominal area of the specimen. The axial concrete capacity was dependent on the compressive strength of the concrete; consequently, the total initial vertical load varied for each specimen. After the axial load was applied, a reversed-cyclic load was added by the eight horizontal actuators under drift ratio control. First, the test specimens were subjected to several cycles of small drift ratios for warming up. Then, the tests were performed by using the loading history consisting of the following drift ratio cycles: 0.1%, 0.15%, 0.25%, 0.37%, 0.5%, 0.75%, 1.0%, 1.5%, and 2.0% (Fig. 10).

3.2. Analytical model

The specimens were modeled using the finite element mesh illustrated in Fig. 11. For each specimen, the cylindrical wall of the vessel was defined by 40 CSMM-based shell elements. Ten layers of concrete and two layers of reinforcing steel were assigned for each element using the corresponding constitutive material modules. The steel layers were defined at the exact locations of the steel in the cross section of the specimen. In Specimen No. 1, all shell elements were assigned with 2% of reinforcement in both the vertical and horizontal directions. The percentage of steel used in shell elements of Specimen No. 2 was almost identical to Specimen No. 1, except the shell elements located within the distance of one-fourth of the net height at the top and bottom of the specimen were assigned with 4% of vertical reinforcement. The top block of each RCCV specimen was defined as a rigid body by using ten 8-node linear-elastic shell elements with high stiffness. For the boundary conditions, all nodes at the bottom of the model were constrained to prevent any translations or rotations. Equal horizontal and

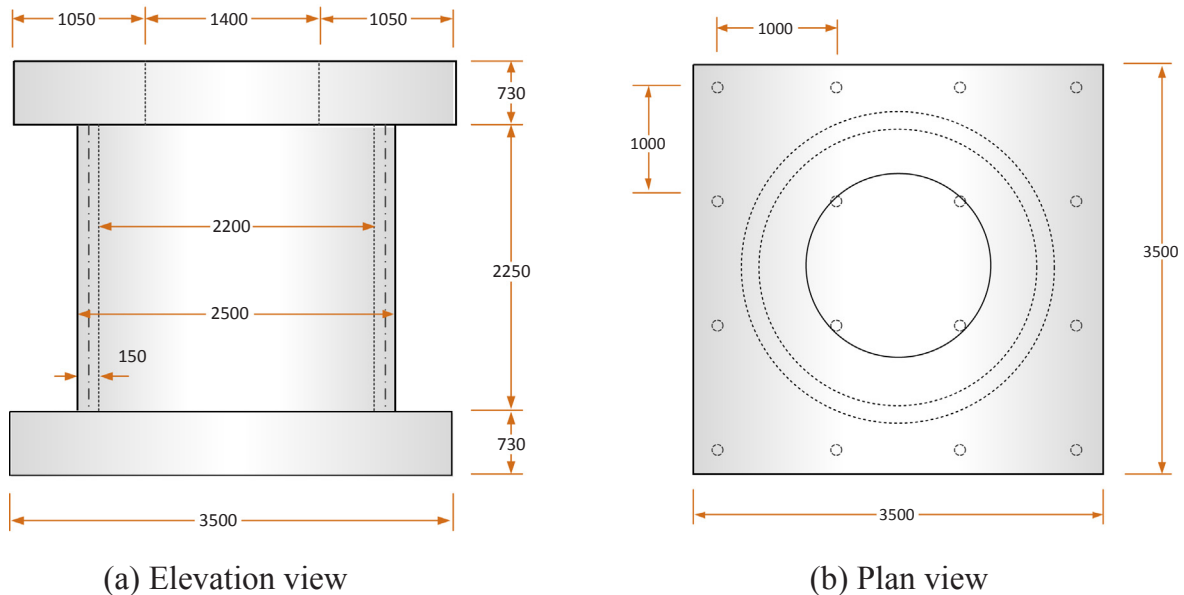


Fig. 7. Dimensions of the RCCV specimens.

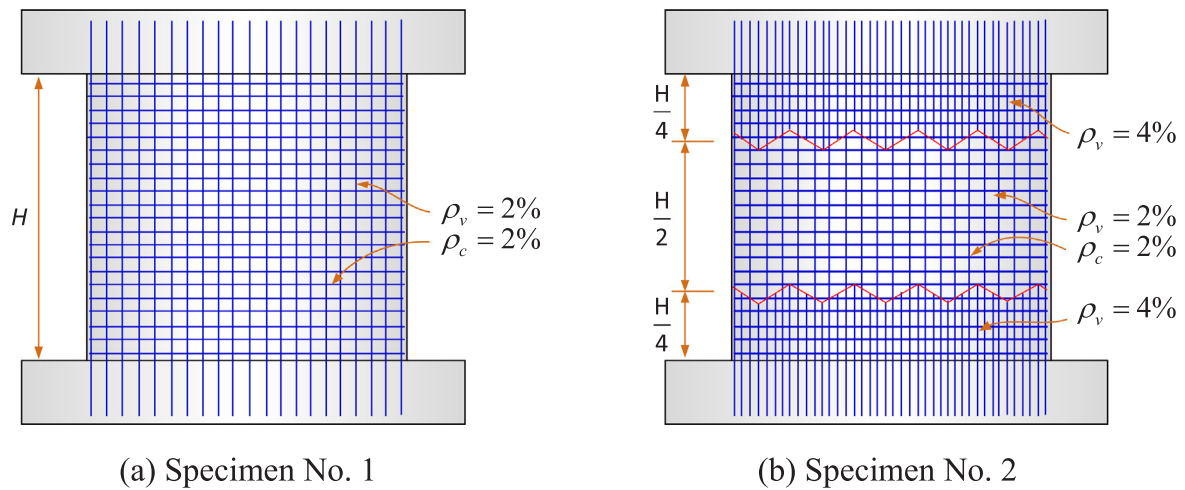


Fig. 8. Reinforcement detail of the RCCV specimens.

vertical loads were applied at all nodes along the perimeter at the height level of the specimen based on the assumption that the loads were uniformly distributed. The axial loads acting on the cap were applied with the direction and magnitude of the loads remaining constant in the analysis. The horizontal loads were changed according to the displacement control scheme.

3.3. Analytical algorithm

The analysis was performed by a predetermined force control for vertical actuators and displacement control schemes for horizontal actuators. The analysis procedure was separated into two steps. In the first step, axial loads were applied to each specimen using load control by ten load increments, i.e. 10% of the total load was applied for each increment. In the second step, axial loads were kept constant and reversed cyclic horizontal loads were applied by the predetermined displacement control on the drift of the specimen. The common displacement increment used in the analysis was 0.5 mm. The solution procedure in the algorithm used the Newton-Raphson method with Krylov acceleration technology [31]. The nodal displacement and corresponding horizontal load were recorded at each converged displacement step, and the stress and strain of the elements were also monitored.

The Cyclic Softening Membrane Model used for the shell element was developed based on a smear cracking model approach to accurately predict flexural and shear behavior. The CSMM does not account for a sliding shear failure that was considered to be a local failure and should be simulated by a discrete model approach. For the purpose of making accurate predictions for the analytical simulation in terms of the sliding shear, an analytical algorithm with an additional sliding shear checking condition was proposed in this study (Fig. 12). The checking condition is based on the sliding shear failure mechanism stated by Paulay, Priestley [32]. Based on this mechanism, when the flexural cracks have not occurred at the junctions of the vessel and the top block, the shear

force from the top block is transmitted to the vessel through the entire cross section of the vessel. After several cycles, flexural cracks occur throughout the entire cross section at the junction of the vessel and the top block, and the shear force is transferred across the flexural compression zone. Before the cracks close to form the compression zone, the shear force is carried mainly by the dowel action of the vertical reinforcement. When all of the vertical reinforcement within the compression zone of the current cycle has yielded in tension from the previous cycle, the compression zone cannot be formed before the shear force reaches the dowel capacity of the vertical reinforcement. As a result, when the shear force exceeds the dowel capacity, shear sliding failure will occur. The analytical algorithm requires the program users to examine the stress and strain diagram of the vertical reinforcement at the junction of the vessel with the top and bottom block to determine if all of the vertical reinforcement within the compression zone of the current cycle has yielded in tension from the previous cycle in order to specify the step at which the sliding shear failure may happen. If the checking condition is satisfied, the current shear force will be compared with the sliding shear limit, which is the dowel capacity of the vertical reinforcement, taken as $0.4A_{sv}f_y$, where A_{sv} and f_y are the total cross-sectional area and the yielding strength of the vertical steel bars, respectively. If the shear force exceeds the dowel capacity, shear-sliding failure will occur.

4. Comparisons of analytical and test results

The experimental and analytical horizontal load versus drift ratio relationships of the test specimens are shown in Fig. 13 and Fig. 14, respectively. The analytical results were obtained from blind analyses conducted before the tests. These curves illustrate the load resisting mechanism of the nuclear containment vessels. Five critical points were indicated in the horizontal load versus drift ratio curve representing the first cracking of concrete (Point 1), the first yielding of vertical and horizontal steel bars (Point 2 and Point 3) and the peak loads in the

Table 1
Dimension and material properties of the RCCV specimens.

Specimen No.	f'_c (MPa)	D (mm)	H (mm)	t (mm)	Vertical Reinforcement			Horizontal Reinforcement		
					f_y (MPa)	f_u (MPa)	ρ_v (%)	f_y (MPa)	f_u (MPa)	ρ_h (%)
RCCV #1	37.0	2350	2250	150	379	572	2.0	376	565	2.0
RCCV #2	43.4	2350	2250	150	379	572	2.0 (4.0)	376	565	2.0

Note: f'_c = Compressive strength of concrete; D = Diameter (Center-to-center); t = Thickness; H = Net height; f_y = Yielding strength of steel; f_u = Ultimate strength of steel; ρ_v = Steel ratio in vertical direction; ρ_h = Steel ratio in horizontal direction.

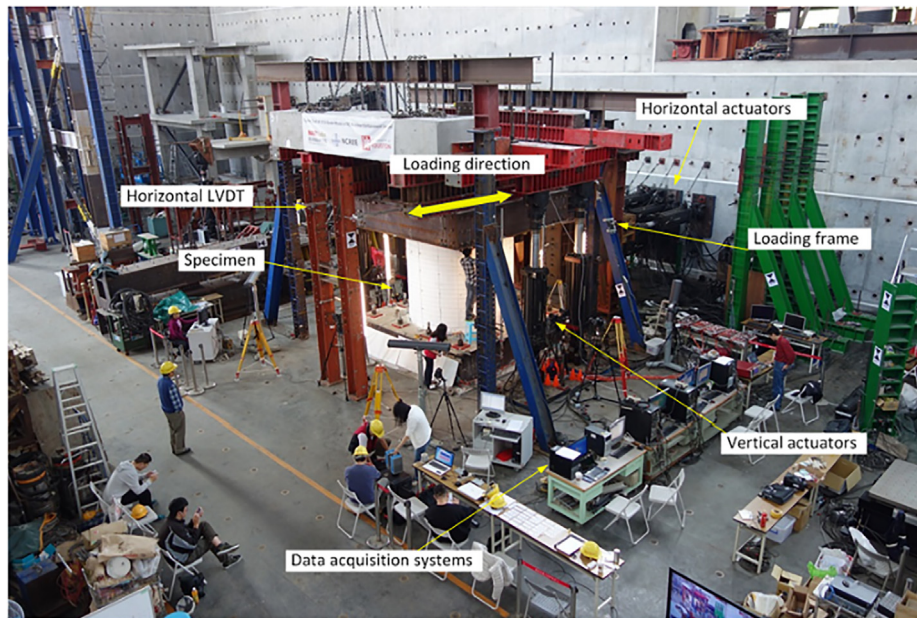


Fig. 9. Overview of test setup.

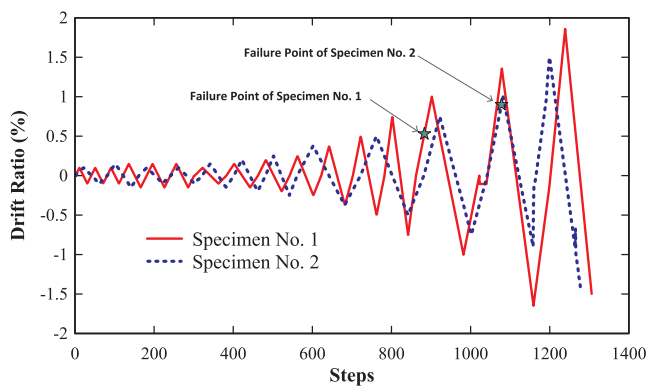


Fig. 10. Loading histories of the specimens.

positive and negative directions (Point 4 and Point 5) in each specimen. The values of the load and drift ratio at the critical points of the specimens are summarized in Table 2. Overall, the analytical results had a good correlation with the experimental data. The analytical model accurately predicted the structural behaviors in both the positive and

negative directions, including the primary backbone curve, the first cracking, the initial stiffness, the yielding distribution of steel bars, and the unloading and reloading paths as well as the pinching effect of the specimens.

4.1. Cracking prediction

The slope of the envelope curve often decreased when the stiffness of the specimen was reduced significantly after cracking (Fig. 13 and Fig. 14). The load and drift ratio of the specimens at the first cracking are shown in Table 2. The experimental cracking loads of Specimen No. 1 and Specimen No. 2 were determined to be 1993 kN and 2095 kN, respectively. The analytical cracking loads were slightly smaller than the cracking loads obtained from the tests. The analytical cracking loads of Specimen No. 1 and Specimen No. 2 were 1445 kN and 1458 kN, respectively. The first cracking happened earlier in the analytical results than in the test outcomes because the first cracking of material constitutive laws (CSMM) in the analytical models was defined based on the occurrence of micro cracks rather than physical cracks that can be observed by eyes. The analytical model can be used for crack control, which is extremely important to prevent the leaking of harmful

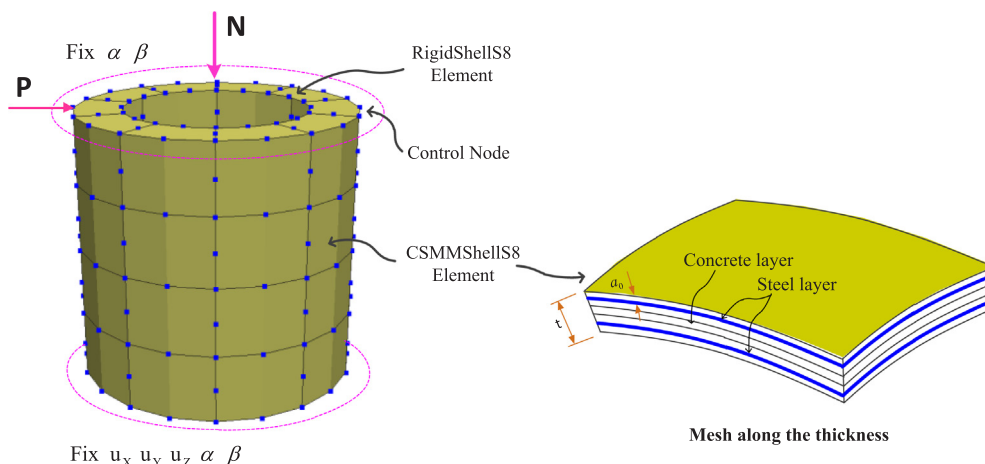


Fig. 11. Finite element model of RCCV specimens.

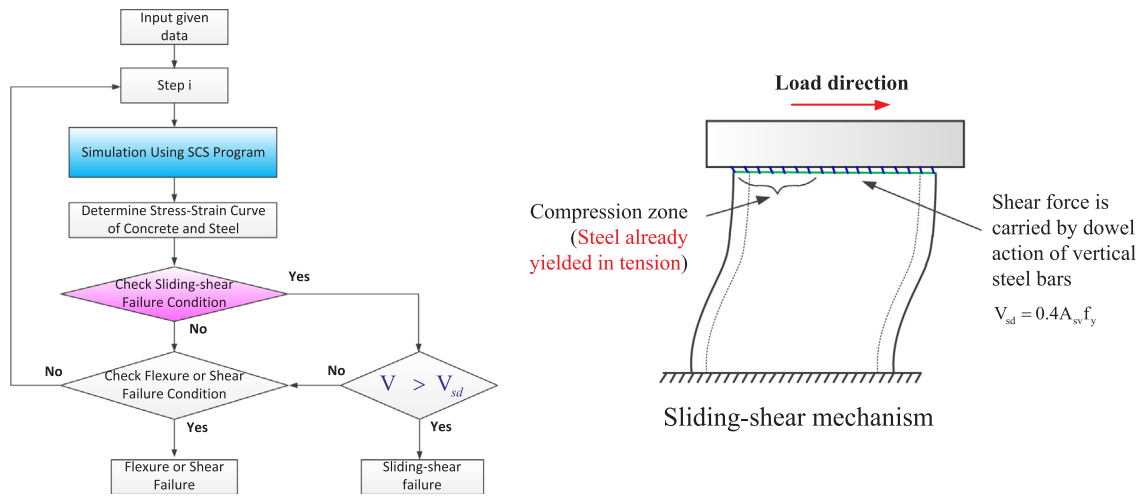


Fig. 12. Analytical algorithm with sliding checking condition.

radiation during a rare nuclear meltdown accident.

4.2. First yielding prediction

When observing the strain data of all the steel bars at each step of loading, it was shown that both the vertical and horizontal steel bars of Specimen No. 1 yielded during the tests. The horizontal steel bars yielded first at the load of 1324 kN and the drift ratio of 0.093% and the vertical steel bars yielded later at the load of 2144 kN and the drift ratio of 0.155% (Table 2). Similarly, in Specimen No. 2, both the vertical and horizontal steel bars also yielded during the test, and the horizontal steel bars reached yield before the vertical steel bars. The horizontal steel bars yielded at the load of 3338 kN and the drift ratio of 0.276% and the vertical steel bars yielded at the load of 4426 kN and the drift ratio of 0.427%.

In the analytical model, the yielding condition of steel bars can be predicted by investigating the values of the stresses and strains of vertical and horizontal steel bars during analysis. Similar to the test results, the analytical results showed that the vertical and the horizontal steel bars of the specimens yielded under the applied loading history (Fig. 14). However, the predicted load and drift ratio at the first yielding are quite different compared to the experimental data. The analytical model predicted that the first yielding points of the vertical and horizontal steel bars were close to each other; however, the vertical steel bars yielded slightly earlier. In Specimen No. 1, the vertical steel bars yielded at the load of 3827 kN and the drift ratio of 0.347% and the

horizontal steel bars yielded at the load of 3927 kN and the drift ratio of 0.36%. In Specimen No. 2, the vertical steel bars yielded at the load of 4161 kN and the drift ratio of 0.316% and the horizontal steel bars yielded at the load of 4327 kN and the drift ratio of 0.333%. It is noted that the first yielding point predictions are based on smeared strains while the first yielding points of the experimental data are based on local strains. It explains the intricacy in the comparison between the first yielding point predictions and the test data.

4.3. Peak load prediction

The recorded peak loads of Specimen No. 1 were 5580 kN and 4951 kN in the positive and negative loading directions, respectively. The drift ratios corresponding to the peak loads were 0.742% and 0.677% in the positive and negative loading directions, respectively. The recorded peak loads of Specimen No. 2 were 6113 kN and 5182 kN in the positive and negative loading directions, respectively (Table 2). The drift ratios corresponding to the peak loads were 0.899% and 0.731% in the positive and negative loading directions, respectively. The peak loads of Specimen No. 2 were slightly higher than the peak loads of Specimen No. 1 in both loading directions because the compressive strength of concrete used in Specimen No. 2 was higher than that used in Specimen No. 1. In both specimens, the lateral strength dropped significantly after the peak load.

In the positive loading direction, the predicted loads and drift ratios at the peak load of the test specimens exhibited have good correlations

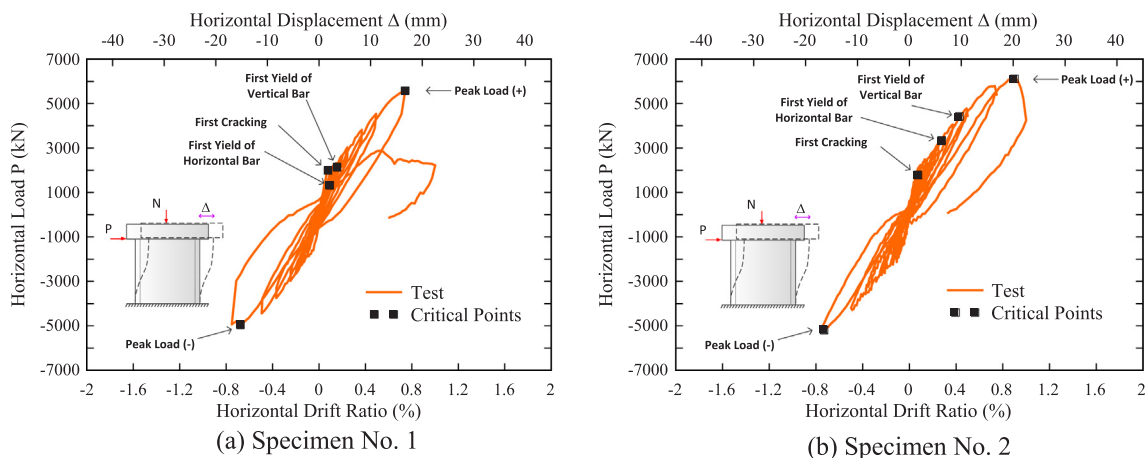


Fig. 13. Experimental horizontal load versus drift ratio relationships.

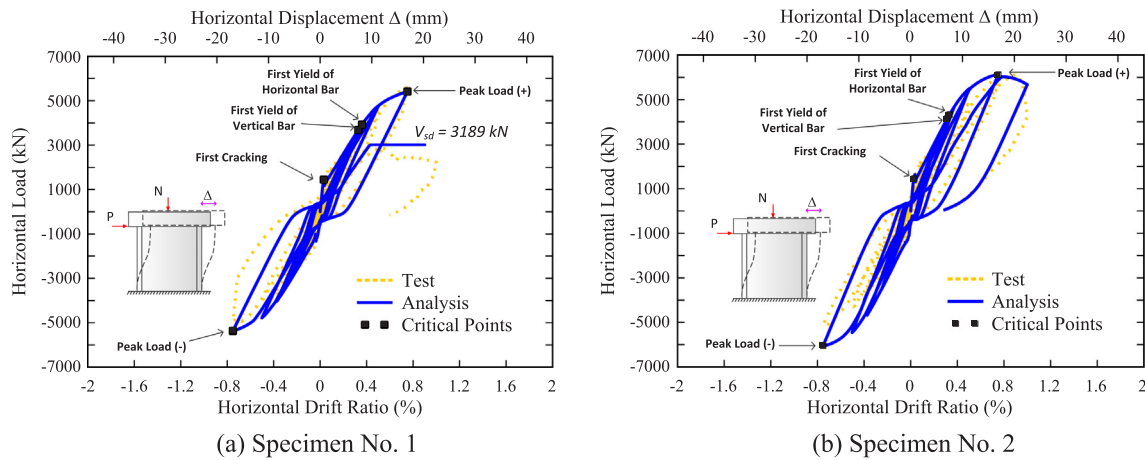


Fig. 14. Analytical horizontal load versus drift ratio relationships.

Table 2
Loads and drift ratios at the critical points of the specimens.

Specimen No.	Δ_{cr} (%)	V_{cr} (kN)	Δ_{yv} (%)	Δ_{vy} (kN)	Δ_{yh} (%)	V_{yh} (kN)	$\Delta_{max}^{(+)}$ (%)	$V_{max}^{(+)}$ (kN)	$\Delta_{max}^{(-)}$ (%)	$V_{max}^{(-)}$ (kN)
1 (Test)	0.077	1993	0.155	2144	0.093	1324	0.742	5580	-0.677	-4951
1 (Analysis)	0.031	1445	0.347	3827	0.360	3927	0.742	5404	-0.751	-5370
2 (Test)	0.073	2095	0.427	4426	0.276	3338	0.899	6113	-0.731	-5182
2 (Analysis)	0.031	1458	0.316	4161	0.333	4327	0.751	6120	-0.751	-6042

Note: V_{cr} , Δ_{cr} = Horizontal load and drift ratio at first cracking; V_{yv} , Δ_{yv} = Horizontal load and drift ratio at first yielding of vertical rebar; V_{yh} , Δ_{yh} = Horizontal load and drift ratio at first yielding of horizontal rebar; $V_{max}^{(+)}$, $\Delta_{max}^{(+)}$ = Horizontal load and drift ratio at peak load in the positive direction; $V_{max}^{(-)}$, $\Delta_{max}^{(-)}$ = Horizontal load and drift ratio at peak load in the negative direction.

with the experimental data, as illustrated in Fig. 14. In the negative loading direction, the analytical results were higher than the experimental results. Table 2 summarizes the analytical values of the load and drift ratio at the peak load of the specimens. For Specimen No. 1, the predicted peak loads were 5404 kN and 5370 kN in the positive and negative loading directions, respectively. The drift ratios corresponding to the peak loads were 0.742% and 0.751% in the positive and negative loading directions, respectively. For Specimen No. 2, the peak loads predicted were 6120 kN and 6042 kN in the positive and negative loading directions, respectively. The drift ratios corresponding to the peak loads were 0.751% in both positive and negative loading directions, respectively.

4.4. Yielding distribution

The experimental yielding distributions of the vertical and horizontal steel bars over the surface of the specimens at the positive peak load are illustrated in Fig. 15. The figure shows that the yielding region of the vertical and horizontal steel bars was spread over a large area on the surface of the specimens. The yielding region formed diagonally from the bottom to the top corners of the specimens (Fig. 15a and Fig. 15b). The yielding region of the horizontal steel bars, however, was concentrated in the mid-height region of the specimens (Fig. 15c and Fig. 15d). The analytical strain distributions of the vertical and horizontal steel bars over the surface of the specimens at the positive peak load are illustrated in Fig. 16. The yielding areas of steel bars obtained from the analysis matched well with the test results. Furthermore, both experimental and analytical results reveal that the specimens have a ductile behavior because the vertical and circumferential steel bars yield significantly before the load reaches its peak value. However, there is no clear yielding plateau existing in the envelope of the load vs.

drift ratio curves of the specimens because the stress and strain of steel bars in many locations still behaved in elastic and the stress values continued to increase. As a result, the load gradually increased from the first yielding point to the peak load.

4.5. Failure mechanisms

It can be observed from the test that the failure modes of the two specimens were very different. Specimen No. 1 failed due to sliding shear that occurred at the top of the specimen (Fig. 17a). The peak load of Specimen No. 1 might have been higher if the sliding shear had not occurred. The sliding shear cracks started to occur on the top of the specimen at a drift of 0.5% and became larger when the load increased. Before the sliding shear failure, no critical damage of the concrete and reinforcement was observed in the specimens. Learning from the failure of Specimen No. 1, additional vertical steel bars, called dowel bars, were added on the top and bottom of Specimen No. 2 to prevent the sliding shear failure. The method was successful because no sliding shear failure occurred and the sliding shear cracks on the top of the specimen were eliminated. As a result, Specimen No. 2 failed when the concrete was crushed in the mid-height region due to web shear failure, and the specimen reached a higher peak load and deformation (Fig. 17b).

Following the proposed analytical algorithm, the stresses and strains of the vertical steel rebars of each specimen were monitored in every step of the analysis. As observed from the analytical results of Specimen No. 1, most of the vertical steel rebars at the top-left corner of the specimen yielded in tension when the specimen reached the peak load in the negative direction (Fig. 18a). These results satisfied the proposed sliding shear checking condition; therefore, the sliding shear failure may occur in the following loading cycle of the specimen. The

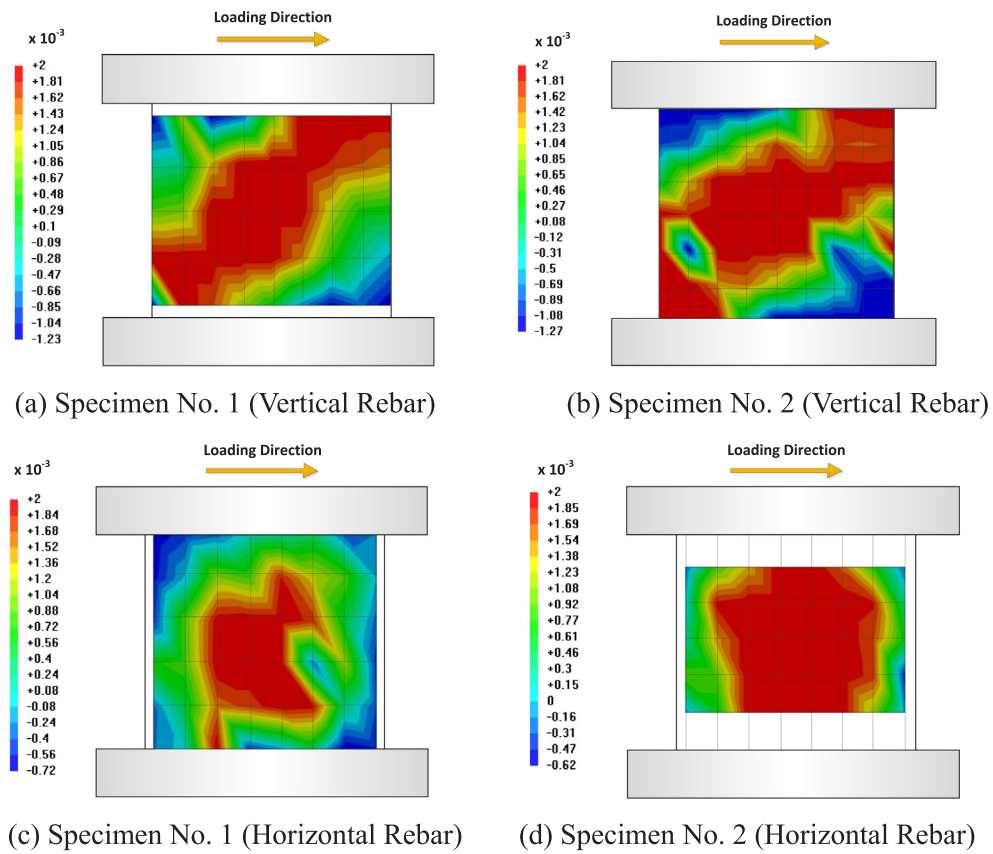


Fig. 15. Contours of experimental strains of steel bars at peak load.

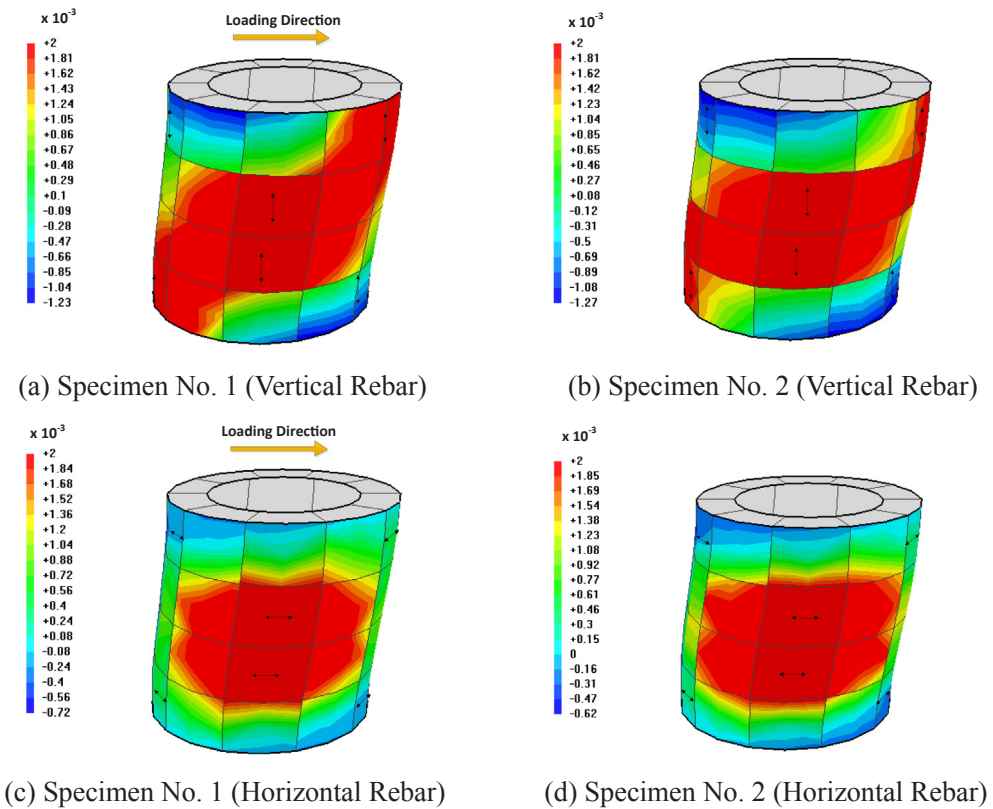


Fig. 16. Contours of analytical strains of steel bars at peak load.

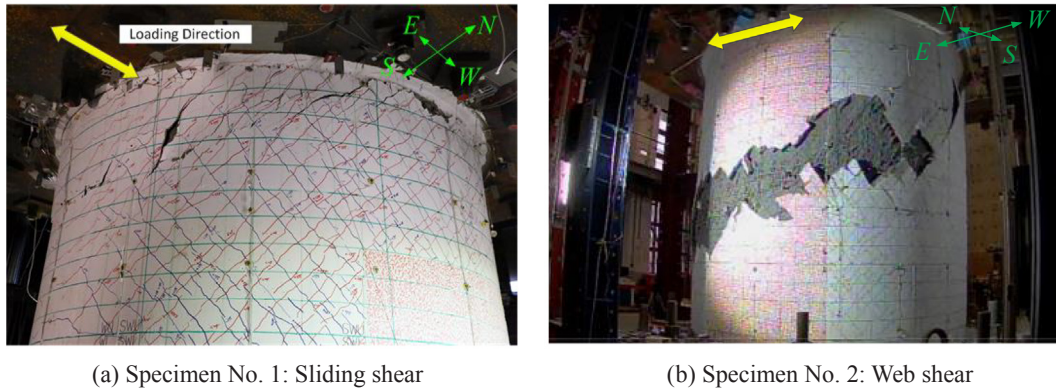


Fig. 17. Failure modes of the RCCV specimens.

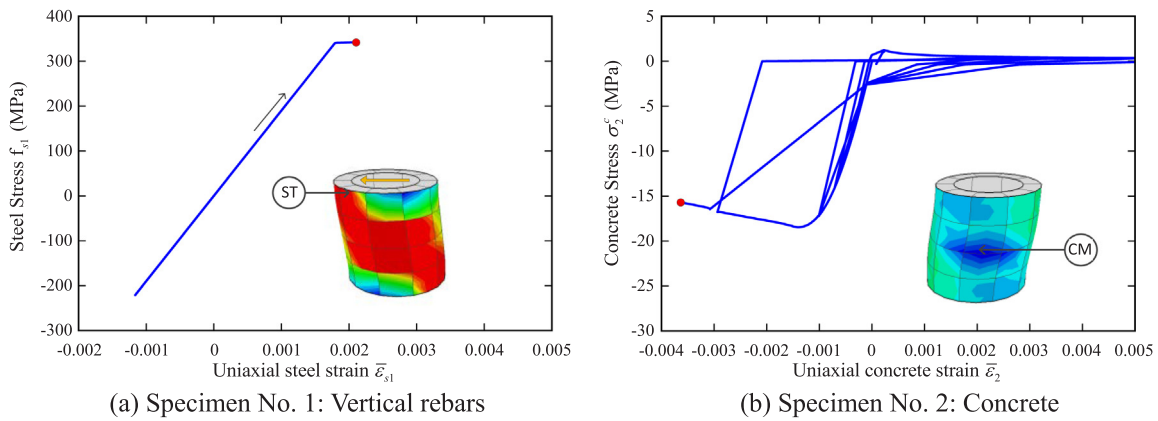


Fig. 18. Stress-strain relationships of materials for explanation of failures.

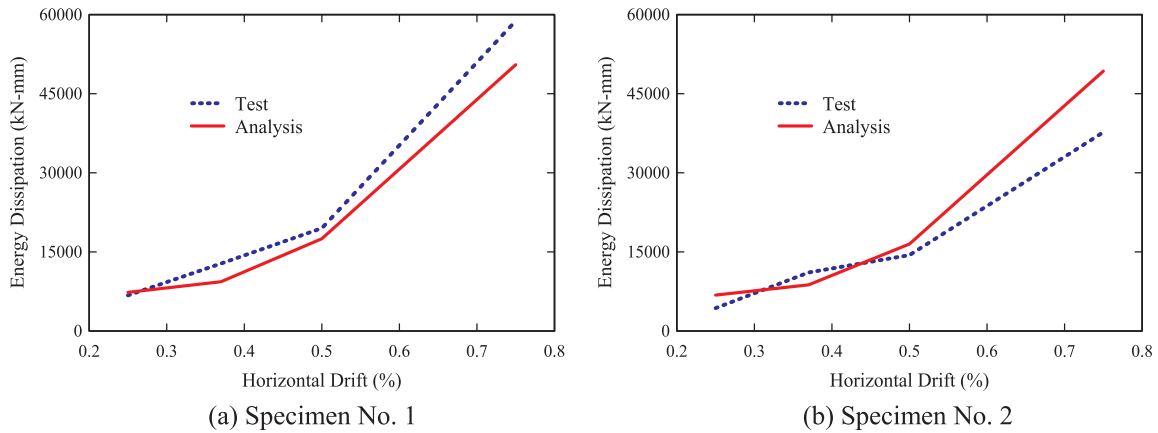


Fig. 19. Comparison of analytical and experimental energy dissipation capacity.

calculated sliding shear limit of Specimen No. 1 was approximately 3189 kN, which was significantly less than the peak load of the specimen. This difference explains why the specimen failed due to sliding shear in the following cycle after the specimen reached the peak load in the negative direction, which is similar to the test results.

Fig. 18b illustrates a typical stress and strain curve of concrete in the principal direction in the mid-height region of Specimen No. 2. just before the load started to drop in the positive direction. The figure shows that the compressive strength of the concrete in the mid-height region was approximately 18 MPa, which was significantly smaller than the compressive strength of concrete, 43.4 MPa. This occurred because the concrete was softened due to the severe opening of the cracks within this region. In addition, Fig. 18b shows that both the stresses and

strains of the concrete in the mid-height region moved further to the descending branch. The result indicates that the concrete in this region was already crushed; therefore, the failure mode of the specimen was web-shear, which is similar to the test results.

4.6. Energy dissipation capacity

Fig. 19 shows the comparisons of the analytical and experimental energy dissipation capacities with respect to the drift loading cycles of the specimens. The energy dissipation capacity of each specimen in a hysteretic loop was calculated by integrating the area surrounded by the hysteretic loop. The energy dissipations were compared up to the maximum drift of 0.75%, which corresponds to the cycle before failure.

As shown in the figure, the energy dissipation capacity of each specimen surged as the drift increased, and the trends of energy dissipation of the specimens could be closely predicted by the analysis results.

5. Conclusion

Two 1/13-scaled cylindrical RC containment specimens were tested at the National Center for Research on Earthquake Engineering (NCREE) to investigate the structural behavior of RC nuclear containment structures under reversed cyclic loading. The tests were undertaken as part of an international collaboration project between the National Center for Research on Earthquake Engineering (NCREE) in Taipei, Taiwan and the University of Houston (UH), Houston, Texas. The nonlinear finite element analysis of the nuclear containment vessel specimens was conducted through the finite element program SCS using the developed CSMM-based shell element. The analytically predicted results compared very well with the experimental data. Overall, the primary backbone curves, the initial stiffness, the peak strength, the descending branch, the yielding distributions and the failure characteristics were accurately predicted. The analytical hysteresis loops also provided accurate measurements of the pinching effect, and the energy dissipation capacity. Hence, the FEA program (SCS) with the developed CSMM-based shell element is a very powerful tool to investigate the seismic behavior of RC containment structures.

Acknowledgement

The research described in this paper is financially supported by the U.S. Department of Energy NEUP program (Project No. CFP-13-5282). The opinions expressed in this study are those of the authors and do not necessarily reflect the views of the sponsor.

References

- [1] Hsu TTC, Wu CL. Cyclic Tests of Cylindrical Concrete Containment Structures and Their 3-D Finite Element Predictions. In: 16th US-Japan-NZ Workshop on the Improvement of Structural Engineering and Resiliency, Nara, Japan; 2016.
- [2] Luu CH, Mo YL, Hsu TTC. Development of CSMM-based shell element for reinforced concrete structures. *Eng Struct* 2017;132:778–90.
- [3] Mansour M, Hsu TTC. Behavior of reinforced concrete elements under cyclic shear II: theoretical model. *J Struct Eng, ASCE* 2005;131:54–65.
- [4] Ahmad S, Irons BM, Zienkiewicz OC. Analysis of thick and thin shell structures by curved finite elements. *Int J Numer Meth Eng* 1970;2:419–51.
- [5] Scordelis AC, Chan EC. Nonlinear analysis of reinforced concrete shells. *ACI Special Publication*; 1987. p. 98.
- [6] Hsu TTC, Wu CL, Lin JL. *Infrastructure systems for nuclear energy*. John Wiley & Sons; 2014.
- [7] Leombruni P, Buyukozturk O, Connor JJ. Analysis of shear transfer in reinforced concrete with application to containment Wall Specimens. Massachusetts Inst. of Tech., Cambridge (USA); 1979.
- [8] Banerjee AK, Holley MJ. Research requirements for improved design of reinforced concrete containment structures. *Nucl Eng Des* 1978;50:33–9.
- [9] Hand FR, Pecknold DA, Schnobrich WC. A layered finite element nonlinear analysis of reinforced concrete plates and shells. University of Illinois Engineering Experiment Station. College of Engineering. University of Illinois at Urbana-Champaign; 1972.
- [10] Cervera M, Hinton E, Hassan O. Nonlinear analysis of reinforced concrete plate and shell structures using 20-noded isoparametric brick elements. *Comput Struct* 1987;25:845–69.
- [11] Hu HT, Schnobrich WC. Nonlinear finite element analysis of reinforced concrete plates and shells under monotonic loading. *Comput Struct* 1991;38:637–51.
- [12] Yamamoto T, Vecchio FJ. Analysis of reinforced concrete shells for transverse shear and torsion. *ACI Struct J* 2001;98:191–200.
- [13] Kim TH, Lee KM, Shin HM. Nonlinear analysis of reinforced concrete shells using layered elements with drilling degree of freedom. *ACI Struct J* 2002;99.
- [14] Maekawa K, Okamura H, Pimanmas A. *Non-linear mechanics of reinforced concrete*. CRC Press; 2003.
- [15] Zhang YX, Bradford MA, Gilbert RI. A layered cylindrical quadrilateral shell element for nonlinear analysis of RC plate structures. *Adv Eng Softw* 2007;38:488–500.
- [16] Lee HP. Shell finite element of reinforced concrete for internal pressure analysis of nuclear containment building. *Nucl Eng Des* 2011;241:515–25.
- [17] Hsu TTC, Mo YL. *Unified theory of concrete structures*. John Wiley & Sons; 2010.
- [18] Collins MP, Vecchio F. The response of reinforced concrete to in-plane shear and normal stresses. University of Toronto; 1982.
- [19] Hsu TT, Belarbi A, Xiaobo P. A universal panel tester. *J Test Eval* 1995;23:41–9.
- [20] Vecchio F, Collins MP. Stress-strain characteristics of reinforced concrete in pure shear. Reports of the Working Commissions. International Association for Bridge and Structural Engineering; 1981. p. 211–25.
- [21] Belarbi A, Hsu TTC. Constitutive laws of softened concrete in biaxial tension compression. *ACI Struct J* 1995;92:562–73.
- [22] Pang XB, Hsu TTC. Behavior of reinforced concrete membrane elements in shear. *ACI Struct J* 1995;92:665–79.
- [23] Pang XB, Hsu TTC. Fixed-angle softened-truss model for reinforced concrete. *ACI Struct J* 1996;93:197–207.
- [24] Hsu TTC, Zhu RRH. Softened membrane model for reinforced concrete elements in shear. *ACI Struct J* 2002;99:460–9.
- [25] Model-Based Zhong J. Simulation of reinforced concrete plane stress structures. Houston: University of Houston; 2005.
- [26] OpenSees. Annual Workshop on Open System for Earthquake Engineering Simulation. Pacific Earthquake Engineering Research Center. UC Berkeley; 2013.
- [27] Cook RD. Concepts and applications of finite element analysis. Wiley. com; 2002.
- [28] Hinton E, Owen DRJ. Finite element software for plates and shells. Swansea, UK: Pineridge Press; 1984.
- [29] Luu CH. Development of CSMM-based shell element for reinforced concrete structures. University of Houston; 2016.
- [30] Batoz JL, Dhat G. Incremental displacement algorithms for nonlinear problems. *Int J Numer Meth Eng* 1979;14:1262–6.
- [31] Carlson NN, Miller K. Design and application of a gradient-weighted moving finite element code I: in one dimension. *SIAM J Sci Comput* 1998;19:728–65.
- [32] Pauly T, Priestley M, Syng A. Ductility in earthquake resisting squat shearwalls. *ACI J* 1982;79:257–69.